ARTICLES
https://doi.org/10.1038/s41929-021-00718-7

nature catalysis

Check for updates

# High-throughput activity screening and sorting of single catalyst particles with a droplet microreactor using dielectrophoresis

Anne-Eva Nieuwelink[1,4], Jeroen C. Vollenbroek[2,4], Roald M. Tiggelaar[3], Johan G. Bomer[2], Albert van den Berg[2], Mathieu Odijk[2] and Bert M. Weckhuysen[1]✉

**Solid catalysts are complex, multi-component materials with large interparticle heterogeneities that hamper statistically relevant in-depth catalyst characterization. Here we introduce an automated high-throughput screening and sorting method for catalyst particles. A droplet microreactor was developed for fluorescence-activated sorting of catalyst particles using dielectrophoresis. Fluid catalytic cracking (FCC) particles stained with styrene derivatives were analysed with the analytical platform developed and sorted based on catalytic activity. Highly active and low-to-moderately active catalyst particles were sorted using 4-fluorostyrene or 4-methoxystyrene as probe, respectively. FCC particles were encapsulated in liquid droplets, where fluorescent FCC particles activated the dielectrophoretic sorter and were sorted within 200 ms. Post-sorting analysis of 4-fluorostyrene-stained and sorted catalyst particles was done using fluorescence microscopy and micro-X-ray fluorescence. This confirmed that the sorted particles were the least deactivated and showed the highest acidity, while non-sorted particles contained more metal poisons.**

Solid catalysts are important materials in the chemical industry and are used to facilitate chemical reactions in an energy-effective and selective way; this is why catalysis is involved in the production of >80% of all chemical products[1,2]. Solid catalysts come in many different shapes and sizes, but what they have in common is that they are often micrometre-sized, structured particles with a well-defined porosity. With increasing knowledge available on the structure, composition and functioning of solid catalysts, we know that these complex, multi-component and hierarchical materials are generally heterogeneous in nature[3,4]. This inter- and intraparticle heterogeneity makes in-depth analysis of the catalyst material difficult by limiting the usability of bulk characterization methods, as well as by complicating single-catalyst particle analysis due to the lack of statistical relevance[5]. Therefore, appropriate techniques should be developed that can perform single-catalyst particle screening in a high-throughput fashion, to provide in-depth information with statistical relevance. In other research fields that deal with large heterogeneous samples, such as biomedical or (bio) chemical screening of cells or proteins, screening and sorting have already been applied. For the analysis and sorting of single cells, the use of microfluidic techniques, such as fluorescence-activated cell sorting (FACS) or magnetic activated cell sorting (MACS), has been investigated extensively, resulting in statistically relevant single-cell analyses[6]. Therefore, FACS and MACS are of interest in regard to single-catalyst particle analysis and sorting.

Microfluidics is a field that involves the manipulation of small liquid volumes—that is, from the microlitre scale down to the attolitre. Typical microfluidic devices have fluidic channel dimensions (width and height) ranging from a few to hundreds of micrometres[7] and are used as analytical devices in chemistry and biology[8,9]. Microfluidic reactors (microreactors) for chemical applications are made using microfabrication techniques essentially derived from the microelectronics industry[10]. The use of chemically inert and optically transparent materials, such as glass, allows chemical analysis within microreactors with optical microscopy or fluorescence and absorption spectroscopy[11]. Integration of sensors and actuators, such as heaters and thermometers, can be used to control temperature in the microreactor[10]. Metallic thin-film microstructures can be used to uniformly (or gradient-wise) heat the microreactor, by means of Joule heating[12–21]. By introducing immiscible liquids inside a microreactor, droplets can be created[22]. Droplets prevent reactant dispersion along the length of the channel (Taylor dispersion)[23] and form an ideal reaction environment because of their well-controlled properties such as shape, size and dispersity, creating a homogeneous reaction environment[24]. Droplets can be used to capture and analyse individual catalyst particles, similar to single-cell analysis[25,26].

Characterization of the multi-component fluid catalytic cracking (FCC) catalyst[1,27,28] would be of great benefit in high-throughput sorting due to its interparticle heterogeneities. FCC is the main chemical process in oil refining for the production of gasoline and propylene, using the residue of crude oil distillation as a feedstock. The FCC catalyst consists of spray-dried porous spheres of 50–150 µm with zeolite as the active phase and AO alumina and clay as matrix[29,30]. The oil is mainly cracked on Brønsted acid sites in the zeolites, but precracking of oil molecules occurs in the matrix material before smaller products enter the crystalline micropores of the zeolite. The zeolites most used in the FCC process are the synthetic ultra-stable zeolite Y (US-Y, FAU) and, to a lesser extent, zeolite ZSM-5 (MFI)[31,32]. The FCC catalyst is deactivated in both a reversible and irreversible manner during the FCC process. Active sites are blocked reversibly by the remaining carbonaceous species

[1]Inorganic Chemistry and Catalysis, Debye Institute for Nanomaterials Science, Utrecht University, Utrecht, The Netherlands. [2]BIOS Lab on a Chip group, MESA+ Institute, University of Twente, Enschede, The Netherlands. [3]NanoLab cleanroom, MESA+ Institute, University of Twente, Enschede, The Netherlands. [4]These authors contributed equally: Anne-Eva Nieuwelink, Jeroen C. Vollenbroek. ✉e-mail: b.m.weckhuysen@uu.nl

on the catalyst, preventing further cracking activity. Therefore, the spent catalyst is regenerated through high-temperature calcination in an oxygen-rich environment, making FCC particles available for consecutive cycles of oil cracking[31]. Irreversible deactivation occurs due to metal accumulation, originating from the oil feedstock, with Ca, Ni, Fe and V being the most notorious. The yield is decreased by promotion of coke formation (Ni and V) and by the creation of a ~1-μm-thick shell on the particle outer surface (Fe and Ca), which reduces porosity[33–43]. Furthermore, the harsh steaming conditions during catalyst regeneration induce dealumination of the embedded zeolite material, thereby decreasing the amount of available Brønsted acid sites. These deactivation processes occur simultaneously during the FCC process. The overall activity in a riser reactor is preserved by continuous replacement of part of the spent catalyst material with fresh FCC catalyst. This leads to a reactor containing a mixture of FCC particles of varying age and degrees of deactivation, called the equilibrium catalyst (ECAT)[27]. The large interparticle heterogeneity of the ECAT complicates its characterization[44]. Both deactivation processes have been thoroughly studied at both the bulk and single-particle level[35,37,45]. Sorting of the FCC ECAT based on density by flotation is used to investigate their deactivation, which is associated with metal loading and catalyst age[46]. Although the flotation method gives a negative correlation between density and catalytic activity, it does not provide insight into the individual role of metals that deactivate FCC particles and is not selective towards zeolite dealumination. The indirect link to deactivation is a severe limitation of this method, since deactivation cannot always be linked to (initial) activity of an FCC particle due to, for example, intrinsic differences after synthesis. Similarly, no trend in the activity of the sorted FCC ECAT particles could be observed using a diagnostic sorting method based on the magnetic moment, and thus Fe content, of FCC ECAT particles[47].

To date, the analysis of single FCC catalyst particles has been focused at the microscopic level, entailing considerable research devoted to mapping the deposition of metals or the change in pore structure with high spatial resolution at the submicrometre scale[39,48]. Although it is very important to gain such in-depth information[5], it is time consuming to perform these synchrotron measurements. Creating a full three-dimensional projection of a single FCC particle can take many hours, excluding data post processing. Therefore, these extensive in-depth analyses[33,39,48] are performed on only a handful of catalyst particles, hampering the statistical relevance of such methods.

Thus it is clear that there is a need for a method or tool that is able to sort ECAT particles by activity. In this study we show that, by using microfluidics for the high-throughput analysis and sorting of catalyst particles, followed by post-sorting analysis of sorted particles, hundreds of catalyst particles can be evaluated more rapidly, gaining valuable information at the single-particle level and adding statistical value to the data obtained.

## Results

**Microfluidic design and sorting of FCC particles.** As mentioned above, the catalytic activity of FCC particles is linked to the availability of (Brønsted) acid sites in their zeolite domains. Therefore, the activity of FCC particles has been visualized using the oligomerization of styrene derivatives, involving acid catalysis at temperatures between 100 °C and 200 °C[49]. Oligomerization products are fluorescent and can thus be characterized with ultraviolet-visible[45] and fluorescence microscopy[50]. In previous work, these two microspectroscopic techniques have been combined to investigate the acidity of different FCC particles with various styrene derivatives as probe molecules[49]. Although the amount of fluorescence produced contains information about particle activity, both techniques are time consuming and have been applied to only a limited number of individual catalyst particles. Fluorescence-activated cell sorting (FACS) systems are available for cell sorting[22,24,51,52], but cannot be directly applied for catalyst particle sorting due to the increased size and density of such particles with respect to cells. In this work a platform has been developed that can be applied to catalyst particle sorting, taking into account certain essential differences with respect to FACS systems. First, catalyst particles for fluidized bed reactors are, by a factor five to ten, larger than biological cells (~10 μm); second, they have a higher skeletal density meaning that they are notably affected by gravity[53]. Due to these differences, the cross-sectional dimensions of the microfluidic channel must be at least 1.5-fold the particle diameter, and precautions have to be taken against particle sedimentation due to gravitational effects. Because the average particle diameter of FCC particles is ~75 μm, the channel depth in the developed microreactor is 150 μm for a width of 390 μm at the narrowest section and 1 mm at the widest. Over the course of the experiments, three sloped channel microreactors were used. An overview of all dimensions of the various features in the microreactor can be found in Supplementary Tables 2 and 3.

For droplet manipulation in microfluidics, various techniques are available using magnetic, pneumatic, thermal, acoustic or electric control to sort droplets of interest from a continuous droplet stream[54]. Active sorting is rapid and droplet response is typically in the order of microseconds to milliseconds. For electromagnetic sorting there are three options[54]. The first is magnetophoresis, which uses the magnetic moment of a particle or droplet to manipulate droplets. The second is electrophoresis, which utilizes an external potential to manipulate charged particles or droplets. The third option is dielectrophoresis (DEP), which uses an electric field gradient to induce a dipole that is based on the contrast in permittivity and conductivity between the droplet (dispersed phase) and medium (continuous phase), as illustrated in Supplementary Fig. 1. Supplementary Table 1 lists the conductivity and permittivity of the liquids used for the continuous and dispersed phases. More details concerning these electromagnetic particle sorting options can be found in Supplementary Information. All the above techniques provide fast feedback, resulting in accurate sorting at high throughput[54]. Because the droplets and particles used in this work were neither inherently charged nor had the same magnetic moment, DEP was used to sort particles and droplets. An example of DEP sorting from the literature is the study of Baret et al. [26], who sorted cells encapsulated in droplets at a throughput of 2,000 $s^{-1}$ with, on average, one cell in every 50 droplets (throughput of 40 cells $s^{-1}$). DEP has been used since the late 1990s to sort and manipulate cells and particles[55]. We refer the interested reader to the principles of DEP sorting in Supplementary Information, where Supplementary Fig. 2 (and corresponding Supplementary Video 2) show early experiments using alternating current (a.c.) DEP sorting of empty droplets. In the present work the DEP technique was used to actively sort droplets containing the most fluorescent particles from a stream that also contained empty droplets and droplets containing low-to-moderate fluorescent catalyst particles. Based on the fluorescence signal obtained from a particle due to the fluorescent probe reaction, a rapid decision must be made on whether to sort the particle or not. Based on sorting zone dimensions (150 μm deep, 1 mm wide and ~4.4 mm long) and an estimated droplet velocity of 20 mm $s^{-1}$, for flow rates between 180 μl $min^{-1}$ and 200 μl $min^{-1}$, this decision has to be made within the order of ~0.2 s. The glass DEP microreactor designed for this task and the process steps used for fabrication are shown in detail in Supplementary Figs. 3 and 4. In the experimental set-up, the fluorescence signal is detected with a photomultiplier tube (PMT) that converts the fluorescence light generated into a voltage; voltage is measured with a National Instruments (NI) myRio data acquisition system (DAQ). Based on the height of the measured voltage, a threshold can be set in the software that is used to determine whether a catalyst particle containing a droplet has to be separated from the bulk stream.

An in-house-constructed set-up is used for the optical detection of fluorescent catalyst particles. Supplementary Fig. 5 shows a conceptual representation of the microreactor and the fluorescent particle detection system. Supplementary Figs. 6, 7 and 8 show a detailed schematic and photographs of the optical/fluidic detection system and electronic processing. Figure 1 combines a conceptual representation and experimental results to explain the aim and sorting principle of the analytical platform developed, starting with the industrial FCC reactor and ending with the fluorescence-based sorting yield of particles encapsulated in droplets using DEP.

Figure 1a shows the deactivation process of FCC particles in an industrial reactor. Fluorescent probes are used to determine particle activity based on the available acid sites (Fig. 1b). The probes used are 4-methoxystyrene, which targets all available acid sites, and 4-fluorostyrene, which targets only the strongest acid sites[50]. Both probe molecules have their own window of operation, as discussed below. Fluorescent catalyst particles stained with 4-methoxystyrene or 4-fluorostyrene, encapsulated in droplets, are flushed through the microreactor while the voltage from the PMT is monitored with the DAQ. In the software a threshold is set at which the DEP electrodes are activated to sort those particles emitting the highest fluorescence signal, as shown in Fig. 1c. Figure 1d shows an image of the microreactor with the fluorescence detection and sorting zone highlighted. A zoom-in of this area demonstrates the sorting principle. The green dashed line highlights the trajectory of an encapsulated FCC particle that begins in the middle of the channel and, when the droplet reaches the detection spot (and the threshold is exceeded) the DEP electrodes are activated (600 V DC (0 Hz) for 95 ms), thereby pulling the droplet towards the sorted outlet (left at the bifurcation). The red dashed line shows the trajectory of another encapsulated particle that does not exceed the threshold, and hence the DEP electrodes are not activated and the droplet flows straight into the non-sorted outlet (right at the bifurcation). These two images consist of multiple frames from a recording in which multiple particles and droplets were recorded. The stability of the droplet stream, meaning that all droplets should flow by default into the non-sorted outlet if no DEP pulse is applied, is verified by determining the position of those droplets in the sorting area close to the bifurcation. For this analysis, droplet morphology and velocimetry (DMV) software, developed by Basu[56], was used; Supplementary Table 4 and Supplementary Fig. 9 show the settings and results of this analysis. Finally, Fig. 1e illustrates the sorting yield of particles successfully sorted using 4-fluorostyrene and 4-methoxystyrene, based on voltage peak height. During these experiments, the outlets of the microreactor are connected to the same reservoir. Multiple videos are recorded for both probe molecules at five different thresholds (that is, two thresholds for 4-methoxystyrene and three for 4-fluorostyrene) to validate whether catalyst particles exceeding the set threshold are indeed sorted, and these particles are labelled as successfully sorted or true positive. Particles that exceed the threshold but flow to the non-sorted outlet are labelled as unsuccessfully sorted or false negative. Finally, catalyst particles below the threshold that follow the path of the empty droplets and are not actively sorted are labelled as successfully non-sorted or true negative, and particles that do not exceed the threshold but flow into the sorted outlet are labelled as unsuccessfully non-sorted or false positive.

For 4-methoxystyrene staining and sorting experiments, two thresholds are used (1.20 V and 1.50 V). Out of 102 catalyst particles, 41 exceeded the threshold value of 1.20 V. From these 41 catalyst particles, 39 were successfully sorted (true positives) whereas two exceeded the threshold but were not sorted into the correct outlet (false negative). Of the 61 non-sorted catalyst particles, 60 did not exceed the threshold and flowed into the corresponding non-sorted outlet (true negatives) while one particle moved into the sorted outlet not having exceeded the threshold, creating a false positive. During this particular experiment, droplet flow was not considered stable and some droplets randomly moved into the sorted outlet (Supplementary Video 4). Despite this instability, all catalyst particles that did exceed the threshold were sorted successfully. The false-positive catalyst particle was in one of the droplets that randomly moved into the sorted outlet. When the threshold was increased to 1.50 V, 13 out of 86 catalyst particles exceeded the threshold; 12 out of 13 were successfully sorted (true positive) and one out of 13 did not flow into the sorted outlet (false negative). No false positives were observed, with the remaining catalyst particles all true negatives and sorted correspondingly. This resulted in sorting yields for the levels of true positives of 95.1% and 92.3%, and for true negatives 98.4% and 100%, for thresholds of 1.20 V and 1.50 V, respectively.

For 4-fluorostyrene staining and sorting experiments, three thresholds were used (0.87 V, 0.95 V and 1.10 V). The total numbers of catalyst particles for each of these thresholds were 5, 16 and 21. Furthermore, sorting yields for true positives and true negatives were all 100% for these experiments. The videos (Supplementary Videos 3–10 can be found as Supplementary Information items while Supplementary Videos 11–29 are available in a repository; Data availability) and additional tables and figures (Supplementary Tables 6 and 7 and Supplementary Fig. 14) on the sorting of these particles can be found in the Supplementary Discussion.

**Fluorescence staining and post-sorting analysis.** The probe 4-methoxystyrene can be oligomerized by all acid sites in the FCC particle, resulting in a large number of fluorescent oligomers with a bright purple colour. An overly high concentration of fluorescent material can lead to self-absorption and quenching of fluorescence, as shown in Fig. 2a. Such highly acidic catalyst particles show low fluorescence. Despite the fact that these particles are sorted correctly based on their fluorescence signal, they can still be labelled as false negatives due to the nonlinear correlation between activity and fluorescence, as indicated in Fig. 2a. As such, the use of 4-methoxystyrene as a probe molecule is applicable in only a relatively small window of operation (compared to 4-fluorostyrene as a

**Fig. 1 | The FCC process, sorting principle and microreactor design. a**, In the FCC process, the catalyst is subject to deactivation. **b**, The activity of FCC catalyst particles can be analysed by fluorescent probe reaction using styrene derivatives that target either all acid sites (4-methoxystyrene) or only the strongest acid sites (4-fluorostyrene). **c**, The stained particles are introduced into a microreactor, which has fluidic channels of 150 µm depth containing a droplet generator, reaction zone and sorting area where the channels have a width of 390 µm, 400 µm and 1 mm, respectively. The microreactor is able to sort the droplets encapsulated in particles based on their fluorescence signal using DEP, where $E$ is the electric field and $F_{DEP}$ is the DEP force with the arrow indicating the direction. The fluorescence signal emitted by particles is detected with a PMT and converted into a voltage. Using a DAQ system, the voltage is recorded. **d**, Based on fluorescence intensity and corresponding voltage signal, a threshold is set which determines whether a particle should be sorted from the main stream or not, where images of the fabricated microreactor and the sorting process show an active particle encapsulated in a droplet (green dashed line) being pulled into the sorted outlet (left at the bifurcation, green box) following activation of the DEP electrodes. The red dashed line shows a particle below the threshold flowing into the non-sorted outlet (right at the bifurcation, red box). In this case, the DEP electrodes are not activated. **e**, Analysis of the sorting process results where the yield of the sorting is shown, indicating the number of particles exceeding the threshold and the subsequent manipulation of those droplets into the sorted outlet for thresholds of 1.20 and 1.50 V, respectively, for 4-methoxystyrene and for thresholds of 0.87, 0.95 and 1.10 V, respectively, for 4-fluorostyrene.

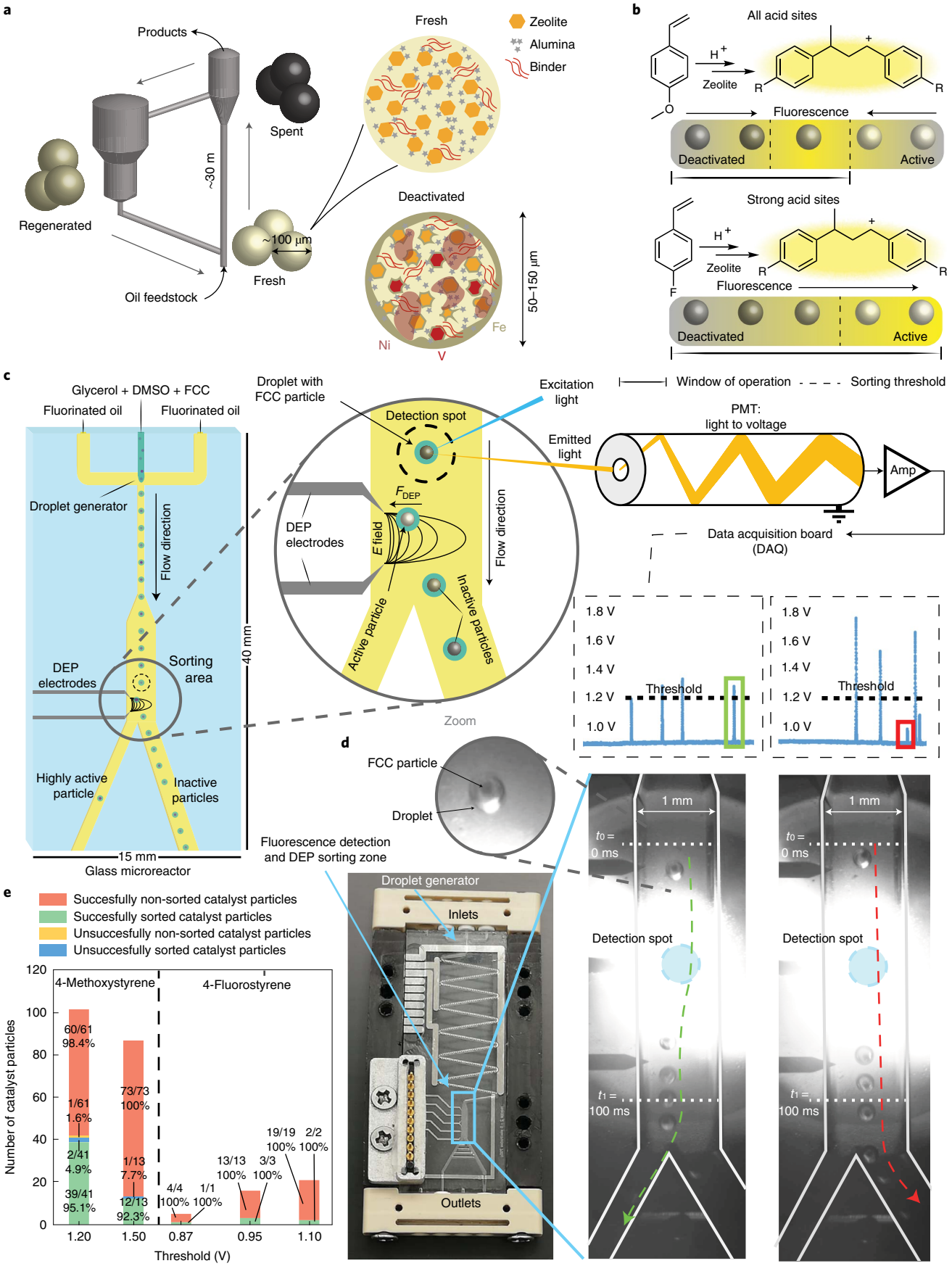
a
Products
Spent
Regenerated
~30 m
Oil feedstock
Fresh
~100 µm
Fresh
Zeolite
Alumina
Binder
Deactivated
50–150 µm
Ni
V
Fe
b
All acid sites
H+
Zeolite
Fluorescence
Deactivated
Active
Strong acid sites
H+
Zeolite
Fluorescence
Deactivated
Active
c
Glycerol + DMSO + FCC
Fluorinated oil
Fluorinated oil
Droplet generator
Flow direction
DEP electrodes
Sorting area
40 mm
Highly active particle
Inactive particles
15 mm
Glass microreactor
Droplet with FCC particle
Detection spot
$F_{DEP}$
DEP electrodes
E field
Flow direction
Active particle
Inactive particles
Zoom
Excitation light
Emitted light
PMT: light to voltage
Amp
Data acquisition board (DAQ)
Window of operation
Sorting threshold
1.8 V
1.6 V
1.4 V
1.2 V
1.0 V
Threshold
d
FCC particle
Droplet
Fluorescence detection and DEP sorting zone
Droplet generator
Inlets
Outlets
1 mm
$t_0$ = 0 ms
Detection spot
$t_1$ = 100 ms
e
Succesfully non-sorted catalyst particles
Succesfully sorted catalyst particles
Unsuccesfully non-sorted catalyst particles
Unsuccesfully sorted catalyst particles
Number of catalyst particles
4-Methoxystyrene
4-Fluorostyrene
60/61 98.4%
1/61 1.6%
2/41 4.9%
39/41 95.1%
73/73 100%
1/13 7.7%
12/13 92.3%
4/4 100%
1/1 100%
13/13 100%
3/3 100%
19/19 100%
2/2 100%
Threshold (V)

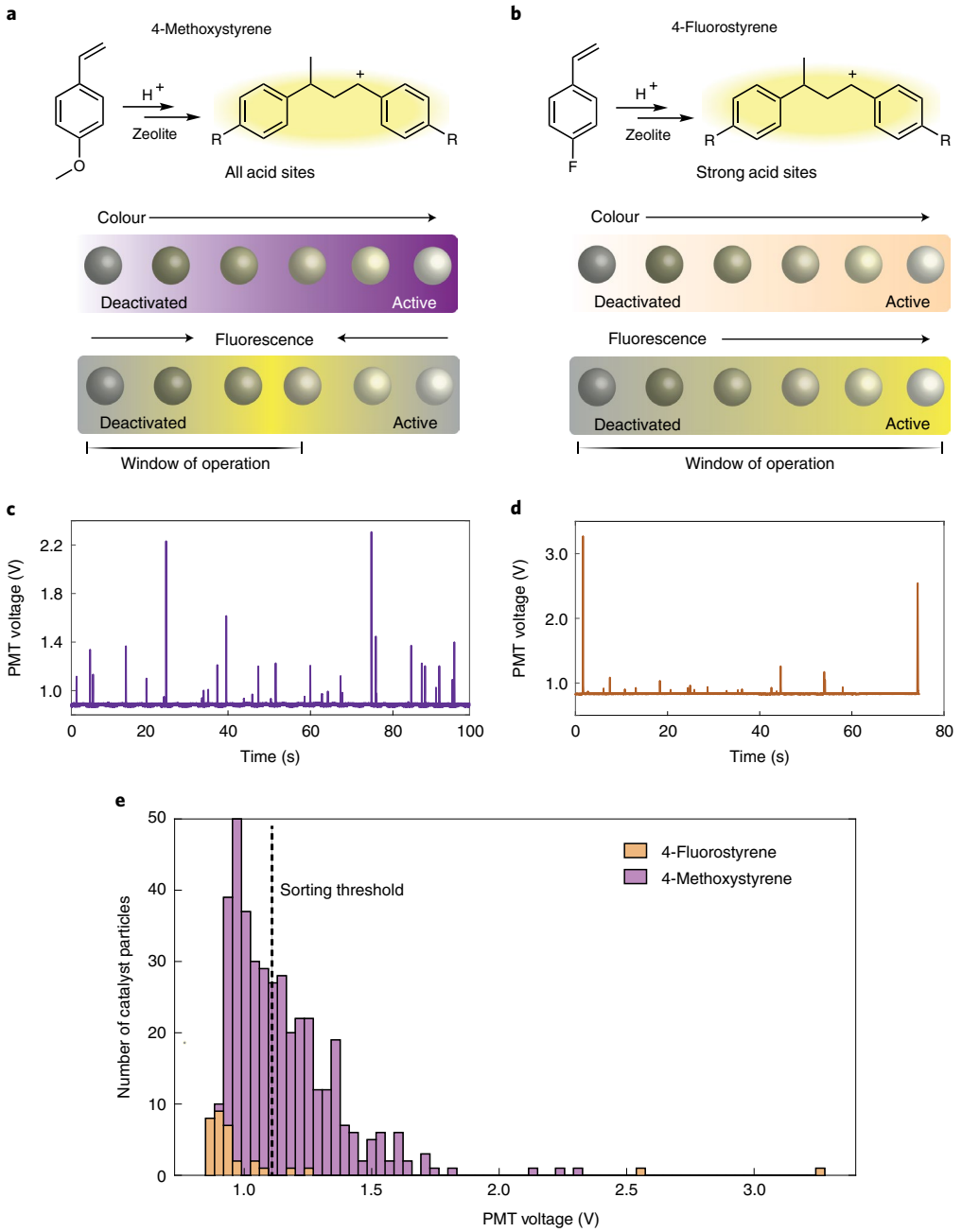


**Fig. 2 | Windows of operation and sorting thresholds for 4-fluorostyrene- and 4-methoxystyrene-stained FCC particles. a**,**b**, The staining principle, including windows of operation for 4-methoxystyrene (**a**) and 4-fluorostyrene (**b**) as probe molecules in the DEP-sorting platform. **c**,**d**, PMT output voltage over time is shown for 4-methoxystyrene (**c**) and 4-fluorostyrene (**d**), where each peak corresponds to a fluorescent particle passing the detection zone. **e**, PMT output values from multiple videos for both probe molecules represented in a histogram, showing peak voltage distribution for 401 particles stained with 4-methoxystyrene (purple) and 33 stained with 4-fluorostyrene (orange). Assuming that total particle population is at least one billion, the 401 detected particles in **e** give a confidence level of 95% with an error margin of 5%, being representative of the entire population.

probe) and, in fact, this probe is suitable for the DEP-based sorting of FCC particles with low to moderate acidity and activity. Further data on the fluorescence and sorting of 4-methoxystyrene particles can be found in Supplementary Fig. 12. A probe that reacts only on highly acidic sites in the FCC catalyst particle is 4-fluorostyrene. This probe forms less fluorescent material with a less distinct visible colour and is therefore not prone to self-absorption and quenching, as shown in Fig. 2b. Consequently, the window of operation of the DEP sorting platform with 4-fluorostyrene as probe is larger compared to 4-methoxystyrene, and it renders it suitable for selective sorting of highly acidic and active catalyst particles. In the Supplementary Discussion a detailed explanation of the window of operation is given, as shown in Supplementary Fig. 13, and additional false negatives due to quenching of the fluorescence. Figure 2c and Fig. 2d show voltage over time for multiple particles stained with 4-methoxystyrene and 4-fluorostyrene, respectively. It is evident that multiple voltage peaks are visible, where each peak corresponds to a passing particle. Recordings were made simultaneously and frames containing a particle were matched with the recorded voltage signal. There is a large variation in the height of

voltage peaks, which corresponds to the large difference in fluorescent product produced by the catalyst particles. In total, 401 catalyst particles stained with 4-methoxystyrene and 33 stained with 4-fluorostyrene were detected during these experiments, resulting in the histogram shown in Fig. 2e. The distribution shows low-to-moderate fluorescence intensity on the left-hand side of the histogram and high intensity on the right. Following comparison with 4-methoxystyrene, for 4-fluorostyrene the distribution is more binary, where only the most active catalyst particles show a strong fluorescence signal because 4-fluorostyrene oligomerizes on only the strongest Brønsted acid sites. As such, there is no mid-section of moderately active particles for 4-fluorostyrene-stained particles. Clearly, the droplet-based microreactor analytical platform can be used for in situ detection of fluorescent light from catalyst particles encapsulated in droplets. Assuming a total particle population of at least one billion, the 401 detected particles in Fig. 2e give a confidence level of 95% with an error margin of 5% in being representative of the entire population. For experiments with both styrene-like molecules, an average high-throughput rate of ~23 droplets $s^{-1}$ was achieved at a total flow rate of ~182 µl $min^{-1}$. The particle influx was not constant: on average every 4 s a particle passed the detection zone, resulting in a fill rate (that is, the percentage of droplets containing a particle) of ~1%.

For 4-fluorostyrene-stained catalyst particles, a sorting threshold of 1.10 V was chosen based on the data shown in Fig. 2e. For this value, a higher number of catalyst particles would be available in the 'sorted' collection container (compared to a threshold of, for example, 1.50 V) for ex situ post-sorting analyses. Particles stained with 4-fluorostyrene that were in situ sorted were then ex situ analysed with fluorescence microscopy and micro-X-ray fluorescence (µXRF) spectroscopy, respectively. This combination of analysis tools was used to determine particle fluorescence intensity and metal content and to find a correlation between fluorescent intensity and the activity/deactivation of these particles. Only 4-fluorostyrene-stained catalyst particles were ex situ analysed in depth, since its oligomerization is more selective for the strongest acid sites, leading to sorting of only the most active catalyst particles. Overlays were made of fluorescence images and µXRF maps, as illustrated in Fig. 3a, which allows individual analysis of all particles: ten sorted particles could be collected and analysed versus 41 non-sorted particles. Correlation analysis is based on segmentation of images and maps after removal of background (Supplementary Fig. 11). This segmentation, however, can result in detection of single particles as multiple domains. Figure 3b shows that catalyst particles from the non-sorted collection reservoir have much lower fluorescence intensity than those in the sorted reservoir. In fact, almost all non-sorted FCC catalyst particles had a substantially lower fluorescent spectrum when compared to sorted particles. Images of sorted and non-sorted particles are shown in Supplementary Fig. 10 (brightness and contrast are enhanced only for enhanced visualization). This lack of fluorescence for non-sorted particles could be due to severe deactivation caused by accumulation of metals such as Ni, Fe, Ca and/or V, or by dealumination of the zeolite domains. Among these metals, Ni is not present in fresh catalyst particles and can therefore be used as a marker for the catalytic age of a particle. It is expected that heavily deactivated particles experienced a longer residence time in the riser reactor unit and therefore had a higher Ni content. Figure 3c shows the metal content of sorted and non-sorted particles. These measurements were performed after segmentation of µXRF maps. With this segmentation, a particle can be represented by multiple segments and the background has been removed. Indeed, particles showing high fluorescence (that is, sorted with the DEP microreactor) have lower Ni and Fe levels, whereas the Ni and Fe contents are high(er) for particles with no/low fluorescence.

One of the particles in the sorted batch exhibited a low fluorescence maximum of 200 counts (Fig. 3b), which is close to that of the particle in the non-sorted batch with the highest fluorescence count. This sorted particle had probably just exceeded the threshold but was not a fresh FCC particle. This was shown by overlaying fluorescence images with the Fe and Ni maps from the same position, as illustrated in Fig. 3a. With this overlay, red–green–blue overlay images as shown in Fig. 3d were formed. It can be seen that particles appearing red have low metal accumulation and vice versa. For example, the particle at far right, appearing green, shows low fluorescence and high Fe content. This is most probably the particle corresponding to the low fluorescence signal in Fig. 3c. A higher sorting threshold would have prevented this partly deactivated particle from being sorted.

Correlative results for metal content were verified using statistical group analysis in SPSS software (Supplementary Table 5). This analysis shows that with the selected sorting threshold, based on correlations between fluorescence and Ni and Fe content, there is an 80% probability that a fluorescent particle contains less Ni or Fe and is, subsequently, sorted in the correct outlet. Therefore, it was concluded that the ECAT particles sorted using this microfluidic DEP platform can be considered to be the least deactivated, demonstrating that the most active catalyst particles can be sorted using this DEP microreactor-based analytical platform for high-throughput fluorescence-activated catalyst sorting.

With this DEP sorting and analysis platform we have a versatile tool that can analyse and sort any catalyst particle provided there is a fluorescent marker. This marker can be sensitive towards acidity, such as 4-fluorostyrene or 4-methoxystyrene, but a larger probe to visualize the porosity of the particle matrix, such as Nile Blue A, can be used with this sorting system[57]. Furthermore, with a slight change in emitted and detected light, we also foresee a possibility for detection and sorting of additives from FCC samples. For example, ZSM-5 FCC particles could be detected by their distinctive pink colour after staining with 4-fluorostyrene[58].

## Conclusions

We have developed a droplet microreactor for high-throughput fluorescence-activated catalyst sorting of ECAT FCC particles using DEP. With this DEP platform it is possible to sort ECAT FCC particles directly related to their activity, something that cannot be achieved with density or magnetic sorting, for example. Particles encapsulated in droplets and stained with two different fluorescent probe molecules (4-methoxystyrene and 4-fluorostyrene) can be detected and sorted in situ at a high-throughput rate of ~23 droplets $s^{-1}$ (0.25 particles $s^{-1}$). By application of DEP, droplets containing highly active catalyst particles, with 4-fluorostyrene as probe, can be manipulated into a sorted outlet that leads to a collection reservoir containing only the most active particles, while less active particles with a low fluorescence signal flow unmanipulated into the non-sorted outlet. Similarly, catalyst particles of low-to-moderate activity can be sorted using 4-methoxystyrene as probe. The yield for catalyst particle sorting was >92% for 4-methoxystyrene-stained particles and 100% for those stained by 4-fluorostyrene. The design default of droplets moving into the non-sorted outlet drastically lowers the likelihood of false-positive results; the only false-positive result occurred when droplet flow—and thus default flow direction—was unstable, essentially eliminating false positives under stable operating conditions. In total, ten catalyst particles stained with 4-fluorostyrene were sorted and found in the sorted collection container. Ex situ analysis with fluorescence microscopy on these ten catalyst particles confirmed that indeed the most fluorescent particles were sorted, while µXRF spectroscopy showed that these particles contained less accumulated metal (that is, Ni and Fe) with respect to unsorted particles. In particular, the presence of Ni in non-sorted particles indicates that the most active particles had been sorted.

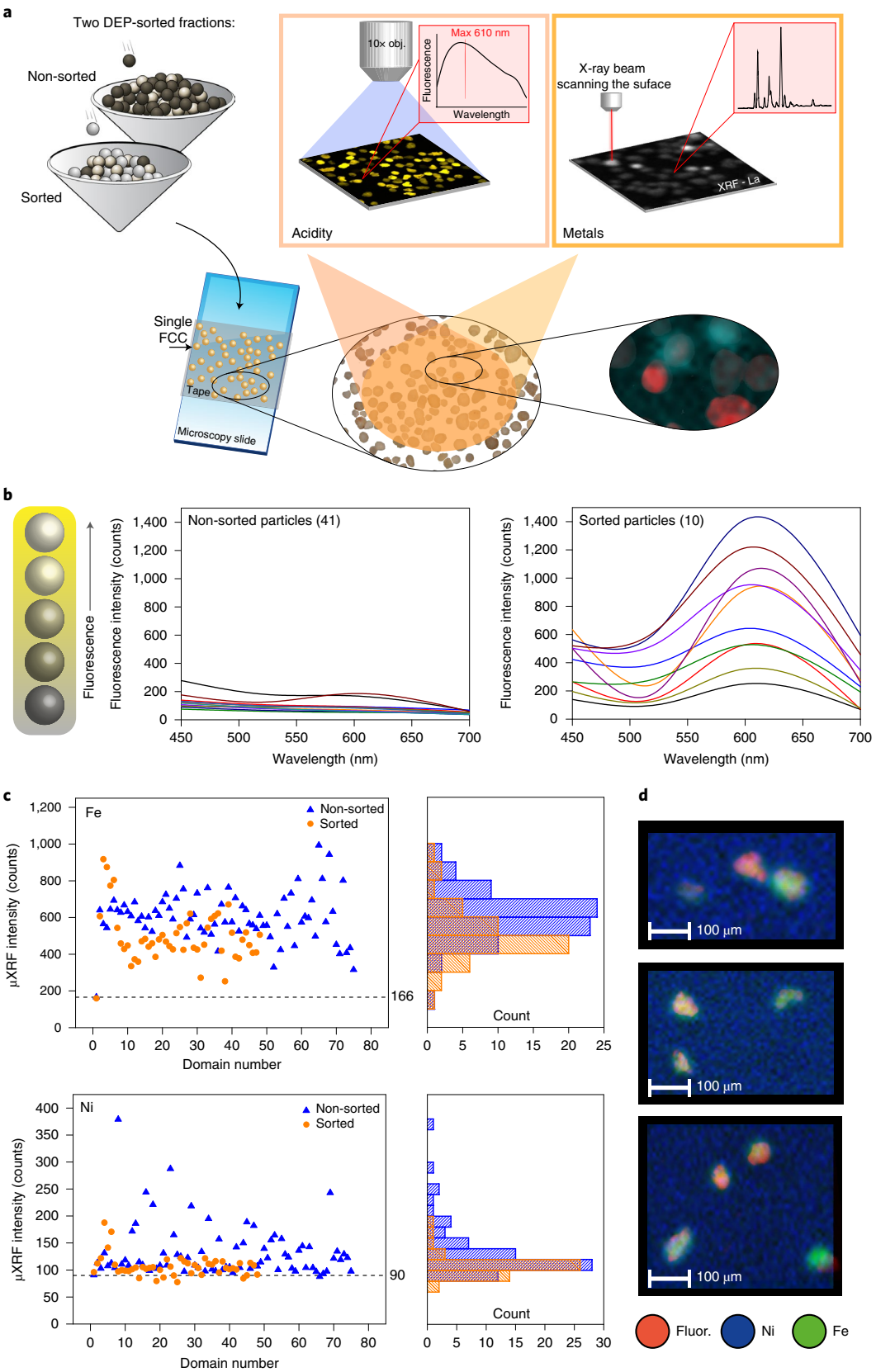


**Fig. 3 | The post-sorting analysis principle of 4-fluorosytrene-stained FCC particles, including data. a**, Post-sorting ex situ analysis process of 4-fluorostyrene-sorted catalyst particles using confocal fluorescence microscopy and μXRF spectroscopy of the 10 sorted and 41 non-sorted particle fractions was performed by transfer of the particles to a piece of tape and subsequent measurement of their acidity and metal content using the aforementioned techniques. **b**,**c**, Fluorescence spectra of non-sorted and sorted particles (**b**) and the μXRF analysis of the Ni and Fe content of the two fractions (**c**). **d**, Overlay of fluorescence images (red) with μXRF maps of Ni (blue) and Fe (green).

By adapting the threshold of this analytical platform to sort only those particles showing the absolute highest fluorescence peaks, it was possible to differentiate zeolite ZSM-5 from zeolite-Y since the former has stronger acid sites than the latter, which means that staining with 4-fluorostyrene is potentially selective for zeolite type. Furthermore, with this fluorescence-activated catalyst sorting DEP-based microfluidic platform, in future research it will be possible to sort and investigate other catalysts. Screening of freshly synthesized catalyst particles can now contribute valuable information on synthesis parameters.

## Methods

**Microreactor design and fabrication.** The glass DEP microreactor (Supplementary Fig. 3) was created using Clewin design software. The dimensions of the various fluidic and electronic features are listed in Supplementary Tables 2 and 3, respectively. The microreactor design has side inlets (and outlets) that are in plane with the flow direction in the microreactor and is based on the 'side-connect' chipholders from Micronit Microtechnologies. This was done to prevent particles from getting stuck in any 90° angle out-of-plane fluidic connections. After the inlets, a droplet generator is included to create droplets in which particles are trapped. The sloped channels in the reaction zone are designed to prevent particles from getting stuck on the channel wall when the microreactor is placed in vertical orientation with the outlets pointing downwards, as shown in Supplementary Fig. 7. In the sorting zone there are needle-like electrodes embedded, the so-called DEP electrodes. Their sharp needle shape is designed to induce a non-homogeneous electric field when a voltage is applied between these needles. After the DEP electrodes the channel branches into two outlets, one for actively sorted droplets (sorted outlet) with highly active particles and the other for bulk droplets containing low-to-moderately active particles or zero particles (non-sorted outlet). The junction of these channels is placed slightly off-centre, with the non-sorted outlet wider (that is, it has lower fluidic resistance) than the sorted, to allow non-sorted droplets to enter the non-sorted outlet by default. There are small slits connecting the two outlets immediately after the junction, to balance potential pressure difference when a droplet enters either of the channels. These slits, also called shunts, have previously been used in droplet sorting by Agresti et al[59]. A droplet entering a channel changes the viscosity of the liquid, which in turn alters fluidic resistance and this affects the pressure drop. These disturbances can make the junction unstable, causing droplets to randomly enter either outlet. By connecting the two outlets with small shunts, pressures between the two outlet channels are linked and junction stability is maintained.

The DEP microreactor was fabricated in the cleanroom of the MESA+ NanoLab at the University of Twente (UT). Supplementary Fig. 4 shows an overview of the process steps. The microreactor is a stack of two 500-µm-thick Mempax glass substrates (diameter 10 cm). A three-mask process is used to fabricate the microreactor. The substrate containing the thin-film electrodes is processed as follows. Buffered hydrogen fluoride (HF) as a wet etchant is used to etch 200 nm into the glass substrate to create the pattern for the Pt structures. This process is followed directly by the deposition of a 10-nm-thick tantalum adhesion layer and a 190-nm-thick Pt layer. All thin-film metallic structures (heaters, temperature sensors and DEP electrodes) are thus embedded in the glass substrate. Subsequently, the glass substrate containing the Ta/Pt structures is covered with a 1.5-µm-thick $SiO_2$ layer deposited with plasma enhanced chemical vapour deposition (PECVD). After deposition, 500 nm is removed from this layer using chemical mechanical polishing to reduce surface roughness. After polishing, a 1-µm-thick (PECVD) $SiO_2$ remains that is sufficiently smooth for fusion bonding. $SiO_2$ is then selectively removed from the contact electrodes. A Cr/Au (5/20 nm) layer is sputtered on the second glass substrate, then photoresist is used to pattern the fluidic channels on top of the Cr/Au layer. The Cr/Au layer is selectively removed with wet etching using a Au/Cr etchant. Subsequently, the fluidic channels are etched 150 µm into the second glass substrate using HF as a wet etchant and the Cr/Au layer as a mask. Etching glass with HF is an isotropic process resulting in semicircular-shaped channels, as shown in Supplementary Fig. 4. Subsequently the Cr/Au mask is removed after HF etching. Electronic accesses are powder blasted from the back surface of the channel substrate, which ensures accessibility of the electrodes embedded in the glass. Finally, the two substrates are bonded using fusion bonding and individual chips are created by means of dicing. The fabrication result can be seen in Supplementary Fig. 3b, in which all fabricated features are indicated.

The holder for the microreactor, as shown in Supplementary Fig. 3b, combines a commercial chip holder enabling side connections (Micronit Microtechnologies) with a home-made chip-holder body made of black Delrin, which is designed with Solidworks and realized by milling (Datron NEO). Small ferrules in the side connector are used to make a leak-free connection between microreactor and tubing.

**Fluorescence detection and sorting set-up.** An in-house set-up is used for the optical detection of fluorescent particles. Supplementary Fig. 5 shows a conceptual representation of the microreactor and the fluorescent particle detection system; Supplementary Fig. 6 shows a detailed schematic of the optical/fluidic detection system and electronic processing, and Supplementary Fig. 7 shows a photograph of part of the laboratory set-up. The inset in Supplementary Fig. 7 shows the microreactor in vertical orientation with the sloped channels. Although this set-up has been reported in previous work[60], some components such as filters, mirrors and excitation sources were changed for this specific application. Droplets containing prestained particles are flushed through the microreactor. On reaching the sorting window, these pass through a detection spot where the excitation wavelength for the fluorescent probe is focused through a ×20 objective (×20/0.4 numerical aperture HCX PL FLUOTAR, Leica). Excitation light is produced with a light-emitting diode (LED) (470 nm, M470L3, Thorlabs) controlled by a LED driver (LEDD1B, Thorlabs). Part of the excitation light (25%) is diverted with a beam splitter (BS019, Thorlabs) to a silicon photodiode (S121C, Thorlabs) connected to a power detector (PM100USB, Thorlabs), to calculate the optical power (3.081 mW) used for the excitation of the sample inside the microreactor. Each particle passing through the detection spot will be excited by the LED light (centre wavelength, 470 nm) and emit light (centre wavelength, 610 nm) at a different wavelength. The emission signal is detected by the objective and is passed through a dichroic mirror (DMLP550R, Thorlabs) and emission filter (MDF620-52, Thorlabs). Another beam splitter (BS013, Thorlabs) directs 50% of the light towards a PMT (H7422, Hamamatsu) that converts the optical signal into a voltage, with 50% directed to a complementary metal oxide semiconductor camera (DC1545M, Thorlabs) used for focusing the detection spot. After amplification (10 V $\mu A^{-1}$) with an amplifier (C7319, Hamamatsu), the voltage can be read out by a DAQ.

A National Instruments (NI) myRio data acquisition board with Labview software installed is used to measure the output voltage of the PMT. The software measures the voltage from the PMT at a sample rate of 1 kHz. In Supplementary Fig. 5 an example is shown of voltage peaks over time, visible when fluorescent particles pass the detection spot. A virtual threshold is indicated, above which the software will immediately activate an electronic switch (Supplementary Fig. 6) that will 'close' (forming an electrical connection) for a specific amount of time that can be set with the software. If the voltage from the PMT is lower than the threshold, the electronic switch is not activated and remains 'open' (forming no electrical connection). The electronic switch is made in-house and is placed in between a function generator (Agilent 33250 A) and a high-voltage amplifier (Trek model 2210). The electric circuit used as the electronic switch to apply the required voltage to the DEP electrodes for DEP activation is shown in Supplementary Fig. 8. The switch control pin of the myRIO is low (0 V) if the threshold for sorting is not exceeded. When the threshold is exceeded and the switch control pin is high (3.3 V), the voltage from the pin is amplified by both −three- and +threefold with two separate operational amplifiers (TL081CP). The outputs of these operational amplifiers (opamps) are connected to the positive and negative power supply pins of a third amplifier (TL081CP). This opamp amplifies the voltage from the function generator with a factor of 10. When the positive and negative power supply pins of this third opamp are −10 and 10 V (this can happen only when the switch control pin is high (3.3 V)), only then the voltage of the function generator is amplified and passed to the high-voltage amplifier (Trek 2210), subsequently activating the DEP electrodes. When the switch is activated, the two systems are connected and the output voltage from the function generator is amplified by the high-voltage amplifier with a factor of 100. The output voltage of the high-voltage amplifier is applied between the DEP electrodes. Initial tests showed that sorting of a droplet using DEP works best when a DC voltage of 600 V is applied for 95 ms between the DEP electrodes. Videos of droplets passing the detection zone are recorded with a PTGREY grasshopper 3 camera (FLIR Integrated Imaging Solutions) at 90 frames $s^{-1}$ and a shutter time of 7.075 ms.

**Detection and sorting of ECAT particles.** A mixture of glycerol and dimethylsulfoxide (DMSO, both Sigma-Aldrich) at a volume ratio of 7:3 is used for the droplet phase and, for the continuous phase, fluorinated FC-40 oil (3 M). An excess of NaCl is added to the droplet phase mixture to increase conductivity and favour the Clausius–Mossotti factor (FCM) at DC (0 Hz) and low-frequency voltages. Supplementary equation 4 shows that conductivity determines the FCM for DC (0 Hz) and low frequencies. After heating the mixture to 80 °C for 10 min, undissolved NaCl is centrifuged out with an Allegra X-12R Centrifuge (Beckman Coulter) and conductivity measured with a conductivity sensor (Seven Multi, Mettler Toledo); this was found to be $22 \times 10^{-3}$ $Sm^{-1}$. All parameters for determination of FCM are given in Supplementary Table 1. With these parameters and for a DC voltage (0 Hz), the FCM has a maximum value of 1 for pDEP.

Calcined FCC ECAT particles are placed on a microscopy slide and heated to 100 °C on a hotplate. Next, 10 µl of either 4-methoxystyrene or 4-fluorostyrene (both 97%, Sigma-Aldrich) is added to the microscopy slide next to the particles. The slide is then covered with a glass Petri dish to allow diffusion of styrene derivatives into the FCC particles. Heating is stopped after 10 s. Staining of FCC particles is performed ex situ.

A Nemesys syringe pump (Cetoni) fitted with a glass Hamilton syringe (5 ml for the continuous phase and 500 µl for the droplet phase) and controlled with Nemesys software is used. Precautions to prevent sedimentation (stirring magnet and vibrational motor) are added to the particle-containing syringe.

Polymer tubing (Tefzel, OD = 1/16", ID = 0.02", Idex HS), in combination with fluidic connectors (Inacom Instruments), is used to connect the syringes to the inlet of the microreactor. The same type of tubing is fitted to the outlets of the microreactor. Both outlets have a separate collection reservoir where filter paper (Whatman 1001-070 grade 1) is used to collect the particles. Before the creation of glycerol/DMSO-in-oil droplets, the channel walls are rendered hydrophobic by flushing the microreactor with a solution of 5.55 µl of tridecafluoro-1,1,2,2-tetrahydrooctyltrichlorosilane (FOTS) added to 1.5 ml of FC-40 oil. Before experiments the microreactor is flushed for 45 min with FOTS/FC-40 solution and then for 45 min with FC-40 only. For the experiments, flow rates of 150–200 µl min–1 for the continuous phase and 1.5 µl $min^{-1}$ for the dispersed phase are used.

**Post analysis of sorted ECAT particles.** FCC ECAT particles exiting the microreactor and collected on filter papers are transferred to a microscopy slide with double-sided tape. Particles are then consecutively analysed by µXRF spectroscopy, optical microscopy and fluorescence microscopy. For µXRF, the microscopy slide is mounted in an Orbis PC SDD with a Rh-tube as X-ray source (30 kV and 200 nA). The surface is scanned with a spot size of 30 µm and step size of 15 µm (300 ms integration time) to obtain an XRF map with optimal intensity per pixel for every element. For optical images, a Zeiss Axio Zoom.V16 microscope using top illumination is used. This microscope is equipped with a PlanNeoFluar Z ×1 zoom objective and an Axiocam 105 colour camera. Fluorescence intensity is measured with a Nikon Eclipse 90i confocal fluorescence microscope with a Nikon Eclipse A1R scan head (×10 objective) equipped with a 488-nm argon ion liquid state Melles Griot laser (40 mW). Data of all three techniques are combined and correlations are made for all particles. Overlaid images are segmented as described in previous research[57], to obtain information for individual particles. The Matlab segmentation is shown in Supplementary Fig. 11. It will be seen that a particle can be divided in multiple domains during segmentation. Most importantly, segmentation allows for background removal.

## Data availability

Supplementary Videos 1–10 are included within the Supplementary information. Supplementary Videos 11–29 can be found in a data repository at https://doi.org/10.24435/materialscloud:em-r4. All data not added to the Supplementary Information or repository are available from the corresponding author on reasonable request.

Received: 25 December 2020; Accepted: 28 October 2021;
Published online: 9 December 2021

## References

1. Boudart, M. in *Handbook of Heterogeneous Catalysis* 2nd edn (eds Ertl, G. et al.) Ch. 1 (Wiley-VCH, 2008).
2. Hagen, J. *Industrial Catalysis* (Wiley-VCH, 2015).
3. Weckhuysen, B. M. Chemical imaging of spatial heterogeneities in catalytic solids at different length and time scales. *Angew. Chem. Int. Ed.* **48**, 4910–4943 (2009).
4. Plessers, E. et al. Resolving interparticle heterogeneities in composition and hydrogenation performance between individual supported silver on silica catalysts. *ACS Catal.* **5**, 6690–6695 (2015).
5. Buurmans, I. L. C. & Weckhuysen, B. M. Space and time as monitored by spectroscopy. *Nat. Chem.* **4**, 873–886 (2012).
6. Sivaramakrishnan, M., Kothandan, R., Govindarajan, D. K., Meganathan, Y. & Kandaswamy, K. Active microfluidic systems for cell sorting and separation. *Curr. Opin. Biomed. Eng.* **13**, 60–68 (2020).
7. Whitesides, G. M. The origins and the future of microfluidics. *Nature* **442**, 368–373 (2006).
8. Auroux, P. A., Iossifidis, D., Reyes, D. R. & Manz, A. Micro total analysis systems. 2. Analytical standard operations and applications. *Anal. Chem.* **74**, 2637–2652 (2002).
9. Reyes, D. R., Iossifidis, D., Auroux, P. A. & Manz, A. Micro total analysis systems. 1. Introduction, theory, and technology. *Anal. Chem.* **74**, 2623–2636 (2002).
10. Jensen, K. F. Microchemical systems: status, challenges, and opportunities. *AIChE J.* **45**, 2051–2054 (1999).
11. Yue, J., Schouten, J. C. & Nijhuis, T. A. Integration of microreactors with spectroscopic detection for online reaction monitoring and catalyst characterization. *Ind. Eng. Chem. Res.* **51**, 14583–14609 (2012).
12. Pattekar, A. V. & Kothare, M. V. A microreactor for hydrogen production in micro fuel cell applications. *J. Microelectromech. Syst.* **13**, 7–18 (2004).
13. Pennell, T. et al. Microfluidic chip to produce temperature jumps for electrophysiology. *Anal. Chem.* **80**, 2447–2451 (2008).
14. Lin, J. L., Wu, M. H., Kuo, C. Y., Lee, K. D. & Shen, Y. L. Application of indium tin oxide (ITO)-based microheater chip with uniform thermal distribution for perfusion cell culture outside a cell incubator. *Biomed. Microdevices* **12**, 389–398 (2010).
15. Crews, N., Wittwer, C., Palais, R. & Gale, B. Product differentiation during continuous-flow thermal gradient PCR. *Lab Chip* **8**, 919–924 (2008).
16. Phatthanakun, R. et al. Fabrication and control of thin-film aluminum microheater and nickel temperature sensor. in *Annual International Conference on Electrical Engineering/Electronics, Computer, Telecommunications and Information Technology* 14–17 (IEEE ECTI-CON, 2011).
17. Miralles, V., Huerre, A., Malloggi, F. & Jullien, M.-C. A review of heating and temperature control in microfluidic systems: techniques and applications. *Diagnostics* **3**, 33–67 (2013).
18. Chang, W.-Y. & Hsihe, Y.-S. Multilayer microheater based on glass substrate using MEMS technology. *Microelectron. Eng.* **149**, 25–30 (2016).
19. Tiggelaar, R. M. et al. Fabrication of a high-temperature microreactor with integrated heater and sensor patterns on an ultrathin silicon membrane. *Sens. Actuators A* **119**, 196–205 (2005).
20. Tiggelaar, R. M. et al. Thermal and mechanical analysis of a microreactor for high temperature catalytic gas phase reactions. *Sens. Actuators A* **112**, 267–277 (2004).
21. Tiggelaar, R. M. et al. Fabrication and characterization of high-temperature microreactors with thin film heater and sensor patterns in silicon nitride tubes. *Lab Chip* **5**, 326–336 (2005).
22. Casadevall, X. Droplet microfluidics: recent developments and future applications. *Chem. Commun.* **47**, 1936–1942 (2011).
23. Kaminski, S. T. S. & Garstecki, P. As featured in: multistep chemical and biological assays. *Chem. Soc. Rev.* **46**, 6210–6226 (2017).
24. Teh, S., Lin, R., Hung, L. & Lee, A. P. Droplet microfluidics. *Lab Chip* **8**, 198–220 (2008).
25. Wen, N. et al. Development of droplet microfluidics enabling high-throughput single-cell analysis. *Molecules* **21**, 881 (2016).
26. Baret, J. C. et al. Fluorescence-activated droplet sorting (FADS): efficient microfluidic cell sorting based on enzymatic activity. *Lab Chip* **9**, 1850–1858 (2009).
27. Cerqueira, H. S., Caeiro, G., Costa, L. & Ribeiro, F. R. Deactivation of FCC catalysts. *J. Mol. Catal. A* **292**, 1–13 (2008).
28. Vogt, E. T. C. & Weckhuysen, B. M. Fluid catalytic cracking: recent developments on the grand old lady of zeolite catalysis. *Chem. Soc. Rev.* **44**, 7342–7370 (2015).
29. Letzsch, W. in *Handbook of Petroleum Processing* Vol. 1 (ed. Treese, S. A.) 262–312 (Springer, 2015).
30. Sadeghbeigi, R. *Fluid Catalytic Cracking Handbook* (Elsevier, 2012).
31. Biswas, J. & Maxwell, I. E. Recent process- and catalyst-related developments in fluid catalytic cracking. *Appl. Catal.* **63**, 197–258 (1990).
32. Komvokis, V., Tan, L. X. L., Clough, M., Pan, S. S. & Yilmaz, B. in *Zeolites in Sustainable Chemistry* (eds Xiao, F.-S. & Meng, X.) 271–297 (Springer, 2016).
33. Wise, A. M. et al. Nanoscale chemical imaging of an individual catalyst particle with soft X-ray ptychography. *ACS Catal.* **6**, 2178–2181 (2016).
34. de Winter, D. A. M., Meirer, F. & Weckhuysen, B. M. FIB-SEM tomography probes the mesoscale pore space of an individual catalytic cracking particle. *ACS Catal.* **6**, 3158–3167 (2016).
35. Mitchell, B. I. R. Metal contamination of cracking catalysts. *Ind. Eng. Chem. Prod. Res. Dev.* **19**, 209–213 (1980).
36. Meirer, F. et al. Life and death of a single catalytic cracking particle. *Sci. Adv.* **1**, e1400199 (2015).
37. Meirer, F. et al. Mapping metals incorporation of a whole single catalyst particle using element specific X-ray nanotomography. *J. Am. Chem. Soc.* **137**, 102–105 (2015).
38. Meirer, F. et al. Agglutination of single catalyst particles during fluid catalytic cracking as observed by X-ray nanotomography. *Chem. Commun.* **51**, 8097–8100 (2015).
39. Kalirai, S., Boesenberg, U., Falkenberg, G., Meirer, F. & Weckhuysen, B. M. X-ray fluorescence tomography of aged fluid-catalytic-cracking catalyst particles reveals insight into metal deposition processes. *ChemCatChem* **7**, 3674–3682 (2015).
40. Liu, Y., Meirer, F., Krest, C. M., Webb, S. & Weckhuysen, B. M. Relating structure and composition with accessibility of a single catalyst particle using correlative 3-dimensional micro-spectroscopy. *Nat. Commun.* **7**, 12634 (2016).
41. Ihli, J. et al. Localization and speciation of iron impurities within a fluid catalytic cracking catalyst. *Angew. Chem. Int. Ed.* **56**, 14031–14035 (2017).
42. Ihli, J. et al. A three-dimensional view of structural changes caused by deactivation of fluid catalytic cracking catalysts. *Nat. Commun.* **8**, 809 (2017).
43. Mathieu, Y., Corma, A., Echard, M. & Bories, M. Single and combined Fluidized Catalytic Cracking (FCC) catalyst deactivation by iron and calcium metal-organic contaminants. *Appl. Catal. A* **469**, 451–465 (2014).
44. Karreman, M. A. et al. Probing the different life stages of a fluid catalytic cracking particle with integrated laser and electron microscopy. *Chem. Eur. J.* **19**, 3846–3859 (2013).

45. Buurmans, I. L. C. et al. Catalytic activity in individual cracking catalyst particles imaged throughout different life stages by selective staining. *Nat. Chem.* **3**, 862–867 (2011).
46. Dyrkacz, G. R., Ruscic, L., Marshall, C. L. & Reagan, W. Separation and characterization of FCC catalysts using density gradient separation. *Energy Fuels* **71**, 849–854 (2000).
47. Solsona, M. et al. Magnetophoretic sorting of single catalyst particles. *Angew. Chem. Int. Ed.* **57**, 10589–10594 (2018).
48. Gambino, M. et al. Nickel poisoning of a cracking catalyst unravelled by single particle X-ray fluorescence-diffraction-absorption tomography. *Angew. Chem. Int. Ed.* **59**, 3922–3927 (2019).
49. Aramburo, L. R. et al. Styrene oligomerization as a molecular probe reaction for Brønsted acidity at the nanoscale. *Phys. Chem. Chem. Phys.* **14**, 6967–6973 (2012).
50. Stavitski, E., Kox, M. H. F. & Weckhuysen, B. M. Revealing shape selectivity and catalytic activity trends within the pores of H-ZSM-5 crystals by time- and space-resolved optical and fluorescence microspectroscopy. *Chem. Eur. J.* **13**, 7057–7065 (2007).
51. Leamon, J. H., Link, D. R., Egholm, M. & Rothberg, J. M. Overview: methods and applications for droplet compartmentalization of biology. *Nat. Methods* **3**, 541–543 (2006).
52. Wolff, A. et al. Integrating advanced functionality in a microfabricated high-throughput fluorescent-activated cell sorter. *Lab Chip* **3**, 22–27 (2003).
53. Huh, D. et al. Gravity-driven microfluidic particle sorting device with hydrodynamic separation amplification. *Anal. Chem.* **79**, 1369–1376 (2007).
54. Xi, H.-D. et al. Active droplet sorting in microfluidics: a review. *Lab Chip* **17**, 751–771 (2017).
55. Fiedler, S., Shirley, S. G., Schnelle, T. & Fuhr, G. Dielectrophoretic sorting of particles and cells in a microsystem. *Anal. Chem.* **70**, 1909–1915 (1998).
56. Basu, A. S. Droplet morphometry and velocimetry (DMV): a video processing software for time-resolved, label-free tracking of droplet parameters. *Lab Chip* **13**, 1892–1901 (2013).
57. Nieuwelink, A.-E. et al. Single particle essays to determine heterogeneities within fluid catalytic cracking catalysts. *Chem. Eur. J.* **26**, 8546–8554 (2020).
58. Kerssens, M. M. et al. Photo-spectroscopy of mixtures of catalyst particles reveals their age and type. *Faraday Discuss.* **188**, 69–79 (2016).
59. Agresti, J. J. et al. Ultra-high throughput screening in drop-based microfluidics for directed evolution. *Proc. Natl Acad. Sci. USA* **107**, 4004–4009 (2010).
60. Van Den Brink, F. T. G. et al. A minaturized push–pull-perfusion probe for few-second sampling of neurotransmittors in the mouse brain. *Lab Chip* **19**, 1332–1343 (2019).

## Acknowledgements

This work was supported by the Netherlands Center for Multiscale Catalytic Energy Conversion, an NWO gravitation programme funded by the Ministry of Education, Culture and Science of the government of the Netherlands. We thank L. I. Segerink and K. Groothuis-Oudshoorn (both University of Twente, UT) for help with SPSS analysis. We thank F. Meirer (Utrecht University, UU) for scientific discussions and help regarding μXRF data analysis. We thank T. Hartman (UU) for the graphical abstract.

## Author contributions

This work is based on a collaboration between the BIOS Lab on a Chip group (UT) and the Inorganic Chemistry and Catalysis group (UU). A.-E.N., J.C.V. and M.O. conceptualized the microreactor and proof-of-principle reaction used in this work and carried out experiments. J.C.V. developed and fabricated the microreactors with help from J.G.B. and R.M.T. A.-E.N. performed ex situ post-sorting analysis. A.v.d.B., M.O. and B.M.W. conceptualized the idea of using microreactor technology for catalyst screening.

## Competing interests

The authors declare no competing interests.

## Additional information

**Supplementary information** The online version contains supplementary material available at https://doi.org/10.1038/s41929-021-00718-7.

**Correspondence and requests for materials** should be addressed to Bert M. Weckhuysen.

**Peer review information** *Nature Catalysis* thanks the anonymous reviewers for their contribution to the peer review of this work.

**Reprints and permissions information** is available at www.nature.com/reprints.

**Publisher's note** Springer Nature remains neutral with regard to jurisdictional claims in published maps and institutional affiliations.